Structural, magnetic, and chemical properties of thin Fe films grown on Rh(100) surfaces investigated with density functional theory

D. Spišák* and J. Hafner
Institut für Materialphysik and Center for Computational Materials Science, Universität Wien, Sensengasse 8, A-1090 Wien, Austria
(Received 25 January 2006; published 25 April 2006)

The structural, magnetic, and chemical properties of ultrathin Fe films grown on Rh(100) films have been investigated using *ab initio* density-functional calculations. The particular interest in this system stems from the fact that in view of the size mismatch between face-centered cubic (fcc) Rh and body-centered cubic (bcc) Fe, it is expected (and actually confirmed by the calculations) that the Fe films will form a tetragonal structure intermediate between bcc α- and fcc γ-Fe, leading to a conflict between the ferromagnetic character of α-Fe and the antiferromagnetism of γ-Fe. Indeed the calculations find a single monolayer of Fe on Rh(100) (which had been characterized on the basis of XMCD experiments as "magnetically dead") to order antiferomagnetically, while thicker Fe films have a ferromagnetic ground state. Independent of the film thickness we find that the magnetic energy differences between the magnetic ground state and possible excited magnetic states are always much smaller than the energy difference between the ground state and the nonmagnetic state. This suggests a lower magnetic ordering temperature than in bulk bcc Fe (in agreement with experiment) and the existence of a disordered local-moment state at higher temperatures. The chemical properties of the films have been tested by the adsorption of CO molecules. We find that the adsorption properties are strongly dependent on the magnetic state of the substrate—the breakdown of magnetic order always leads to a significant enhancement of the adsorption energy. At low coverages we predict the existence of a tilted adsorption geometry similar to that reported for the (100) surface of α Fe.

DOI: 10.1103/PhysRevB.73.155428 PACS number(s): 75.70.Ak

I. INTRODUCTION

The growth of epitaxial films on appropriate substrates is a widely used technique for the stabilization of metastable crystalline phases, which are otherwise not found at room temperature conditions. The material properties of such films can be distinctly different from those of their native bulk phases, if these exist at all. This opens the way towards the design of unique materials with tailor-made properties. Examples are ultrathin magnetic films with a strong perpendicular magnetic anisotropy and hence prospective applications in magnetic information storage technology[1] or bimetallic catalysts consisting of strained ultrathin films on size-mismatched substrates.[2]

Prototypical epitaxially stabilized systems are thin fcc Fe films on various nonmagnetic substrates. Bulk iron in a face-centered cubic (fcc) form (γ-Fe) is thermodynamically stable only above 1184 K where it is paramagnetic. Fe precipitates in a Cu matrix adopt the fcc structure of the matrix and order antiferromagnetically.[3,4] The most common substrate for growing epitaxially stabilized films of γ-Fe is copper because of a proper lattice matching to fcc iron. A large body of experimental and theoretical work has brought ample evidence for a complex correlation between the Fe/Cu(100) film morphology and magnetism.[5–10] The films retain a distorted fcc structure up to a thickness of 11 monolayers (ML). Above this critical thickness a structural transformation from fcc to bcc has been observed. The thinnest films (up to 3 ML) are ferromagnetic (FM), at a thickness of 4 ML a transition to partially antiferromagnetic (AFM) films with "live" ferromagnetic double layers at their surface is observed. The FM films are tetragonally expanded perpendicular to the surface of the films, while the thicker AFM films are isotropically fcc on average. Density-functional calculations[9,10] and low-energy electron diffraction (LEED) experiments[7] agree on an expansion of the spacing between FM coupled layers and a contraction between AFM coupled layers. Also there is an ongoing debate[11] whether Fe/Cu(100) films are grown in a pseudomorphic tetragonally strained (1×1) phase or undergo a complex $(n\times1)$ reconstruction of the near-surface layers reflecting the fundamental instability of face-centered tetragonal Fe along the epitaxial Bain path against monoclinic shearing.[10] Tensor-LEED investigations,[7] atomically resolved scanning tunneling experiments,[8] and *ab initio* calculations[10] agree on $(n\times1)$ reconstructions, $n=4,5$, consisting of monoclinically sheared stripes in the FM regime up to 4 ML, and a (2×1) or (2×2) clock reconstruction in the AFM regime, illustrating the strong correlation between the atomic and magnetic structures of the films. The (1×1) film structures reported very recently on the basis of ion-beam triangulation experiments[11] most likely result from the averaging over large surface areas and shadowing effects (caused by grazing incidence angles of the ion beam).

In addition to the striking contrast in the magnetic properties, α-Fe (bcc) and γ-Fe (fcc) display distinctly different chemical properties. While bcc Fe is located at the limit between the transition metals which dissociate CO and those on whose surfaces only molecular adsorption is observed [as signaled by a tilted adsorption geometry on[12–17] α-Fe(100)], only molecular adsorption in an upright geometry has been reported for ultrathin films of γ-Fe.[18–21] High resolution electron energy loss (HREELS), near-edge x-ray adsorption fine structure (NEXAFS) and temperature-programmed desorption (TPD) experiments have shown that on the bcc

Fe(100) surface CO adsorbs in three states, from which the strongly tilted configuration—tilt angles relative to the surface normal between $45° \pm 10°$ (Ref. 13) and $55° \pm 2°$ (Ref. 16) have been reported—in the hollow site with both oxygen and carbon ends bound to the iron surface atoms is the most stable, while the less strongly bound states have been assigned to CO adsorbed at bridge and top sites. The tilted state in the fourfold hollow is a precursor for the CO dissociation observed at 440 K.[12–16] The saturation coverage of CO on α-Fe(100) is 0.5 ML. In contrast, at 90 K CO molecules adsorbed on near-fcc Fe/Cu(100) films populate bridge sites at low coverage and top sites with increasing coverage.[19] At room temperature a $c(2\times2)$ overlayer structure has been observed with CO filling merely bridge sites.[20] This observation agrees with our previous study based on DFT calculations[21] predicting bridge-adsorbed CO at half-monolayer coverage on a 4-ML thick Fe/Cu(100) films, independent of the magnetic state. At about 370 K CO desorbs without dissociation from the surface.[18]

The extensively investigated Fe/Cu(100) films are (at least on average) close to the fcc structure in the thin film limit, or close to the bcc structure for films exceeding the critical thickness for the fcc/bcc structural transition. It is hence of evident interest to study the magnetic and chemical properties of films on substrates with a more pronounced size-mismatch leading to a films structure intermediate between these two limits. A continuous variation of the in-plane lattice constant in Fe films can be achieved by deposition on the (100) surface of disordered Cu_xAu_{1-x} alloys.[22] The average magnetic moment of films deposited on these substrates increases with the lattice parameter. On a $Cu_3Au(100)$ substrate (lattice parameter $a=3.75$ Å, compared to $a=3.61$ Å for copper) the fcc-like phase is stabilized only up to a thickness of about 5 monolayers,[23] thicker films revert to a bcc structure. Fe films on noble metal surfaces [Ag(100) with[24,25] $a=4.09$ Å or[25,26] Au(100) with $a=4.08$ Å] assume a bcc structure because of excellent matching along the fcc Ag(Au)[110]‖bcc Fe[100] azimuth. There are also several studies of iron films on Rh, Pd, and Pt surfaces, motivated partly by the desire to investigate the magnetic moments induced in nonmagnetic transition metals by the proximity to a ferromagnet. The lattice parameters of these metals are in such a range ($a=3.80$, 3.89, and 3.92 Å for Rh, Pd, and Pt, respectively) that both bcc and fcc iron phases are strained in plane, the former is under a compressive strain whereas the latter under a tensile strain. It is evident that the films are tetragonally distorted (assuming a pseudomorphic growth), however, it is less clear whether they should be considered as bcc-like or fcc-like. This question is particularly important for Fe/Rh(100) films, as some authors[27] reported the absence of FM ordering up to 6 ML and suggested the possibility of an AFM phase, conceivable for a nearly fcc structure. Later experiments using spin and angular resolved x-ray photoelectron diffraction and magnetic circular dichroism[28–30] found FM order above a coverage of 2 ML and the initial film structure has been described as a fct structure evolving into a bct structure above 6 ML with the magnetic moment reaching that of bcc iron. The Curie temperature of the FM films was found to be strongly thickness dependent, varying between about 100 K for 2-ML films and 800 K for 5-ML films. A significant amount of alloying near the interface prevents preparation of pure ultrathin[31,32] Fe/Pd(100) and Fe/Pt(100) films.[33] Thicker films on these substrates assume a bcc structure. In contrast, no notable degradation of interface by intermixing has been encountered for Fe/Rh(100) films.[34] The growth mode of Fe/Rh(100) films has been studied by Pfandzelter *et al.*[35] by grazing incidence scattering of the atoms, confirming epitaxial, pseudomorphic growth which proceeds layer-by-layer at first, followed by multilayer growth on top of a 2-ML film.

A complimentary characterization of the films is provided by adsorption studies. Very recently, chemisorption of CO on Fe/Rh(100) films has been studied via the spectroscopy of the adsorbed molecules.[36] Three molecular adsorption states have been reported on 1 ML Fe film with two sharp and one weak loss peaks at 2060 cm^{-1}, 1950 cm^{-1}, and 1630 cm^{-1} in the HREEL spectrum assigned to top, bridge, and hollow sites, respectively. For films with 2 to 3 ML Fe the two sharp peaks merge into a broad maximum at 2000 cm^{-1}. With further increasing film thickness the position of the high-frequency band shifts slightly below 2000 cm^{-1}, and the intensity of the low-frequency mode assigned to hollow-adsorbed CO relatively increases. TPD of CO saturated films produces three molecular desorption peaks and one recombinative desorption peak, similar as on the (100) surface of bcc Fe. However, it is not clearly established whether CO adsorbed at fourfold hollows dissociates on heating. The saturation coverage of CO on Fe/Rh(100) surface is not known accurately. In all likely hood, the saturation coverage of CO on Fe-capped Rh(100) surfaces is close to the saturation coverage of a clean Rh(100) facet, i.e., about 0.75 ML at 300 K and 0.83 ML at higher temperatures.[37] Similar experiments for NO adsorbed on[36] Fe/Rh(100) produce a distinct N-O stretch mode at 1825 cm^{-1} with a shoulder at 1630 cm^{-1}, tentatively assigned to top and bridge-adsorbed NO. On heating, molecular desorption and dissociation compete. A TPD peak at 350 K is assigned to molecular desorption of NO bound to top sites and at 450 K adsorbed NO is fully dissociated. However, it is now well established that site assignment based on the comparison of the measured molecular stretching frequencies with those known from metal-carbonyl and nitrosyl complexes alone can be misleading.[38–40] Extensive DFT calculations of molecules adsorbed on transition-metal surfaces have shown that the frequency ranges used for site assignment have to be revised.

In the present paper we investigate the structural, magnetic, and chemical properties of 1 to 4-ML thick iron films grown on Rh(100) surface using state-of-the-art *ab initio* density-functional calculations. We examine in detail the correlation between the geometric and magnetic structures of the films. The surfaces of 1 and 4 ML thick films are further explored by the analysis of the adsorption properties of CO molecules in $c(2\times2)$ and (1×1) overlayer structures. The influence of magnetism on the preferred adsorption site and on the vibrational frequencies as well as the demagnetizing effect of the adsorbate are reported. A further purpose of our study is to analyze how the bonding of CO to clean rhodium surface is modified by the presence of an iron capping layer.

The organization of the paper is as follows. Section II contains a description of our computational method. The structural and magnetic properties of thin Fe/Rh(100) films are discussed in Sec. III. Section IV details the results of CO adsorption on surfaces under study. Finally, the main conclusions are summarized in Sec. V.

II. COMPUTATIONAL METHOD

The quantum-mechanical framework of our investigation is density-functional theory within the local density approximation. The calculations performed in this study used the VASP (Vienna *ab initio* simulation program) code.[41] This program performs an iterative solution of the Kohn-Sham equations for periodic boundary conditions. The electronic orbitals are expanded in terms of plane waves with a maximal kinetic energy of 450 eV. The electron-electron interaction is described by projector-augmented wave (PAW) potentials.[42,43] The PAW approach shares the computational efficiency of the pseudopotential approach but is an all-electron technique avoiding the problems related to the linearization of the core-valence exchange interaction.

We use the RPBE exchange-correlation functional[44] which improves the calculated adsorption energies compared to frequently used[45] PW91 or[46] PBE functionals. However, the RPBE functional leads in some cases to a less satisfactory description of bonding in crystals; for fcc Rh we calculate a lattice parameter of $a=3.865$ Å and a bulk modulus $B=233$ GPa. The corresponding values obtained with PW91 functional are $a=3.843$ Å and $B=251$ GPa, i.e., closer to the measured values[47,48] of $a=3.803$ Å and $B=269$ GPa. For bcc Fe, the results are $a=2.872$ Å and $B=131$ GPa (RPBE); $a=2.831$ Å and $B=185$ GPa (PW91); and $a=2.867$ Å and $B=163$ GPa (experiment[47,49]).

Placing a CO molecule in a cubic box with an edge of 20 Å we obtained using the RPBE functional a C-O bond length of $D=1.149$ Å, a vibrational frequency of $\omega=2118$ cm^{-1}, a dissociation energy of $E_d=10.18$ eV, and an electric dipole moment $\mu=0.134$ D. The experimental values[51] are $D=1.128$ Å, $\omega=2143$ cm^{-1}, $E_d=11.2$ eV, and $\mu=0.122$ D.

The Fe/Rh(100) system has been modeled by slabs comprising six Rh layers, one to four Fe layers, and a sufficiently thick vacuum space of 13 Å. For both FM and AFM configurations we used slabs with two atoms per layer, in a $c(2\times2)$ geometry. An adsorbate layer was placed on the top surface of the slab with the C bonding to the metal atoms. VASP allows to calculate the Hellmann-Feynman forces acting on ions, hence a full structural optimization of the adsorbate/film/substrate complex may be carried out. The structural relaxation is completed after all forces, except those acting on atoms in the three frozen layers at the bottom of the slab, drop below 10 meV/Å. Brillouin-zone integrations have been performed via the Methfessel-Paxton technique[52] with a smearing parameter of 0.2 eV and all total energies were extrapolated to zero smearing. We used a grid of $18\times18\times1$ size leading in total to 45 irreducible k points for the surfaces with fourfold symmetry and to 81 irreducible k points for surfaces with a twofold symmetry, i.e., those covered by CO molecules in bridge sites. The vibrational frequencies for CO were obtained by diagonalizing the dynamic matrix set up with force constants determined from the energy variation caused by displacements of C and O atoms by ±0.02 Å in the respective directions. The Rh atoms were assumed to remain stationary as they are about eight times heavier than the C and O atoms.

TABLE I. Structural and magnetic properties of 1-ML Fe/Rh(100) films: contraction Δd_{ij} of the interlayer distances (in pct. of the interlayer distance $d_0^{[100]}=1.93$ Å in fcc rhodium), distance $\bar{d}$ of the Fe layer from the substrate, magnetic moments m_i (the subscript i numerates atomic layers from the surface), and magnetic energy differences ΔE (per Fe atom) relative to the ground-state configuration. In-plane antiferromagnetic (AFM), ferromagnetic ($u|$Rh), and nonmagnetic (NM) solutions have been considered.

	AFM	$u\|$Rh	NM
ΔE (meV)	0	28	820
$m_1(\mu_B)$	±3.00	3.03	0.00
$m_2(\mu_B)$	±0.06	0.27	0.00
Δd_{12}	−12.6	−7.2	−17.2
Δd_{23}	4.6	2.3	5.8
Δd_{34}	0.0	0.0	−0.2
$\bar{d}$ (Å)	1.68	1.78	1.59

III. IRON FILMS OH Rh(100)

We start by considering films consisting of one to four layers of iron grown epitaxially on the Rh(100) substrate. Tables I–IV summarize the structural, energetic, and magnetic properties of these films. We have explored various possible magnetic configurations: ferromagnetic (FM), in-plane antiferromagnetic (AFM) [i.e., with opposite magnetic moments on nearest-neighbor sites in the same (100) plane

TABLE II. Calculated structural and magnetic properties of 2-ML Fe/Rh(100) films, see Table I. Here $\bar{d}$ stands for the average interlayer distance between the Fe layers, and between the Fe film and the top layer of the substrate and $\overline{c/a}$ denotes the average axial ratio in the Fe film.

	$uu\|$Rh	AFM	$du\|$Rh	NM
ΔE (meV)	0	103	179	521
$m_1(\mu_B)$	2.97	±2.74	−2.75	0.00
$m_2(\mu_B)$	2.73	±2.14	2.56	0.00
$m_3(\mu_B)$	0.25	±0.05	0.22	0.00
Δd_{12}	−14.3	−20.9	−10.7	−30.5
Δd_{23}	−5.2	−7.4	−6.7	−23.2
Δd_{34}	1.8	2.2	2.5	0.7
Δd_{45}	0.2	0.3	−0.1	0.5
$\bar{d}$ (Å)	1.74	1.65	1.76	1.61
$\overline{c/a}$	0.90	0.85	0.91	0.83

TABLE III. Calculated structural and magnetic properties of 3-ML Fe/Rh(100) films, see Tables I and II. The "mixed" magnetic configuration refers to in-plane AFM order in the Fe interface layer and ferromagnetism at the free surface, cf. text.

	uuu|Rh	mixed	AFM	*duu*|Rh	*udu*|Rh	NM
ΔE (meV)	0	40	95	97	214	531
$m_1(\mu_B)$	2.92	2.99/2.85	±2.80	−2.92	2.72	0.00
$m_2(\mu_B)$	2.51	2.39/2.28	0.00	−2.31	−2.00	0.00
$m_3(\mu_B)$	2.72	−2.71/2.53	±2.73	2.59	2.67	0.00
$m_4(\mu_B)$	0.26	−0.06/−0.14	0.00	0.22	0.19	0.00
Δd_{12}	−18.9	−12.1/−22.2	−28.1	−20.5	−14.2	−30.4
Δd_{23}	−15.4	−13.6/−13.6	−13.0	−9.9	−8.8	−10.5
Δd_{34}	−6.8	−11.6/−5.5	−8.7	−6.5	−6.3	−11.7
Δd_{45}	2.4	3.0/3.0	3.2	2.3	2.4	3.4
$\bar{d}$ (Å)	1.66	1.68	1.60	1.69	1.73	1.59
$\overline{c/a}$	0.86	0.87	0.83	0.87	0.89	0.82

around any atom], mixed ferro/antiferromagnetic configurations consisting of sequences of FM planes with alternating orientations of the magnetic moments in planes [we use the notation $u(d)$ for planes with all moments directed upwards (downwards)], and nonmagnetic (NM).

A. Magnetic structure

For a 1-ML Fe/Rh(100) we found that the in-plane AFM structure of the Fe overlayer with atomic moments of $\pm 3\mu_B$ has the lowest energy. The magnetic moments in a FM configuration are of the same size, but this configuration is disfavored by 28 meV/Fe atom, while the nonmagnetic solution is 820 meV/Fe atom higher in energy. In all thicker films the FM solution represents the ground state and the first metastable solution is the in-plane AFM configuration whose energy is about 100 meV/Fe atom higher. Our result supports the conclusions drawn by Hayashi *et al.*,[28] who observed ferromagnetism only in films with more than 2 ML. This agrees with our prediction of an in-plane AFM ground state for Fe monolayers on Rh(100). The absence of magnetic ordering in 2-ML thick films might be attributed to a low Curie temperature as the reported measurements have been conducted at room temperatures.

TABLE IV. Calculated structural and magnetic properties of 4-ML Fe/Rh(100) films, see Tables I and II.

	uuuu|Rh	AFM	NM
ΔE (meV)	0	117	493
$m_1(\mu_B)$	2.94	±2.83	0.00
$m_2(\mu_B)$	2.42	±0.11	0.00
$m_3(\mu_B)$	2.58	±2.36	0.00
$m_4(\mu_B)$	2.72	±2.45	0.00
$m_5(\mu_B)$	0.25	±0.05	0.00
Δd_{12} (Å)	−18.5	−25.7	−31.5
Δd_{23} (Å)	−18.1	−14.9	−7.4
Δd_{34} (Å)	−14.5	−15.1	−24.6
Δd_{45} (Å)	−6.8	−8.0	−5.7
Δd_{56} (Å)	2.5	3.2	1.7
$\bar{d}$ (Å)	1.64	1.62	1.59
$\overline{c/a}$	0.85	0.84	0.82

For the ferromagnetic films with two or more ML we calculated magnetic moments of about 2.95 μ_B for the Fe surface layer and 2.72 μ_B for the Fe layer at the Fe/Rh interface, magnetic moments of Fe in the inner layers range around 2.5 μ_B. The magnetism of the in-plane AFM films displays a complex pattern: surface and interface moments are slightly smaller than in the FM configuration, but the most striking feature is that the magnetic moment in the subsurface Fe layer is completely quenched for 3-ML films and extremely weak in 4-ML films. This indicates a conflict between the in-plane AFM induced by Fe/Rh interactions across the interface (see also below) and the native FM of the Fe layers uninfluenced by the proximity of the Rh substrate. To examine this point further, we have investigated a "mixed" magnetic phase with in-plane AFM at the interface and FM order at the free surface (see Table III). Indeed such a configuration turns out to be metastable, with a total energy intermediate between the FM and AFM configurations. This result underlines that due to competing exchange interactions, different magnetic phases with small energy differences coexist in Fe/Rh(100) films. Hayashi *et al.*[28–30] have measured the magnetic circular dichroism (MCD) near the Fe $2p$ adsorption edge and used the sum rule for MCD to evaluate the spin magnetic moment and the ratio of orbital and spin moments. For films with six and more ML, the spin moment at room temperature ranges around $2.2\mu_B$, this is almost the same value as in bulk bcc Fe. For thinner films, the measured room-temperature moments drop dramatically and vanish at about 2 ML. Curie temperatures are strongly reduced compared to bulk bcc Fe, for 4-ML films T_c is about 530 K, decreasing linearly with decreasing film thickness and vanishing for films with less than 2 ML. Since the magnetization of ultrathin films is known to decrease linearly with increasing temperature on approaching T_c (Ref. 50), the

measured room-temperature moments are necessarily significantly lower than the saturation moments resulting from the DFT calculations. Such a reduction of T_c with decreasing film thickness has also been observed in Fe films grown in Ag(100) substrates.[53] In the present case the decrease of T_c is even more pronounced, because in the monolayer limit, AFM and mixed magnetic configurations become comparable in energy with the FM state.

The magnetic moments induced by the proximity effect in the top layers of the Rh substrate are rather weak. The proximity effect is most pronounced for FM overlayers where we calculate induced moments of about $0.25\mu_B$, while for an in-plane AFM interface layer, the induced moments drop to $\pm 0.06\mu_B$. Much larger induced moments have been reported for Fe/Rh multilayers,[54] reaching about $1\mu_B$ in the limit of thin Rh spacer layers squeezed between rather compact Fe layers.

B. Geometric structure

The tetragonal film structure shows a rather complex dependence on the thickness and on the magnetic order in the films. For 1-ML Fe/Rh(100) films the Fe-Rh interlayer distance is 1.59/1.68/1.78 Å for NM/AFM/FM Fe layers (to be compared with 1.93 Å in bulk Rh), indicating a rather pronounced magnetovolume effect. In thicker Fe/Rh(100) films the average interlayer distance shows a similar dependence on the magnetic order, for 4-ML films we find 1.59/1.62/1.64 Å for NM/AFM/FM films. However, the tetragonal distortion of the films is not homogenous: the surface layer always relaxes inwards, in layered magnetic structures distances between ferromagnetically coupled layers are always larger than distances between antiferromagnetically coupled layer—quite analogous to our earlier results on Fe/Cu(100) layers. The experimental results on the film structure are scarce and rather conflicting. Begley *et al.*[55] used quantitative LEED analysis to determine individual interlayer distances. For a single Fe ML they reported a Fe-Rh distance of $d_{\text{Fe-Rh}}=1.74\pm0.03$ Å which is slightly larger than the 1.68 Å we find for the stable AFM phase. For a 2-ML film, the LEED results are $d_{\text{Fe-Rh}}=1.78\pm0.03$ Å and $d_{\text{Fe-Fe}}=1.73\pm0.03$ Å. Our calculations for the FM film predict a more pronounced inward relaxation of the surface layer (1.65 Å) and a slightly larger Fe-Rh distance (1.83 Å), but again the agreement is reasonable. For the 3-ML film the LEED results are 1.74/1.64/1.66 Å (all ±0.03 Å), starting from the interface, to be compared with 1.80/1.63/1.56 Å from DFT for a FM phase. Hayashi *et al.*[28] used x-ray photoelectron diffraction to determine the average interlayer distance as a function of film thickness. They reported an interlayer distance of 1.53±0.05 Å in the initial growth stage, increasing with increasing film thickness and reaching a constant value of 1.66±0.06 Å at a thickness of 6 ML. This trend agrees with our DFT results if one admits that the 1 and 2 ML films are nonmagnetic at room temperature, while the 3 and 4 ML films are already ferromagnetically ordered, see the parameter $\bar{d}$ in Tables I–IV: 1.59 Å (NM 1 ML), 1.61 Å (NM 2 ML), 1.66 Å (FM 3 ML), 1.64 Å (FM 4 ML).

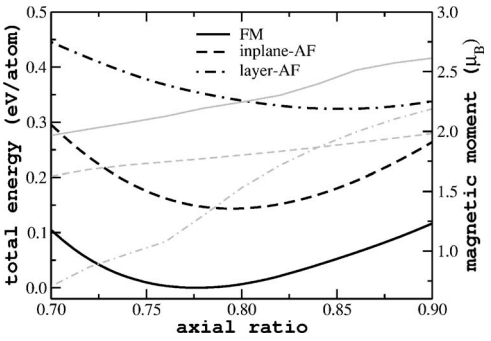

FIG. 1. Total energy and magnetic moment of ferromagnetic and antiferromagnetic face-centered tetragonal Fe constrained to match the lattice parameter of a Rh(100) surface as a function of the axial ratio c/a.

The geometric structure of the films and their ferromagnetic ordering is largely determined by the properties of bulk Fe subject to the epitaxial constraint. Figure 1 shows the variation of the total energy and of the magnetic moments of tetragonal bulk iron with the lattice constants in the basis plane equal to those of the rhodium lattice whereas the intralayer distance along the tetragonal axis varies. It is obvious that independent of the interlayer distances the FM phase is preferred over both layered and in-plane $c(2\times2)$ AFM phases. The total-energy minimum is found for an axial ratio of $c/a=0.78$ (corresponding to an atomic volume of 11.26 Å^3), and the magnetic moment amounts to $2.21\mu_B$. The antiferromagnetic phases are slightly expanded along the tetragonal axis, they also have a lower magnetic moment of about $2\mu_B$ at equilibrium. The expansion is rather modest for the in-plane AFM phase ($c/a=0.80$), and larger for the layered AFM structure ($c/a=0.85$), corresponding to atomic volumes of 11.55 Å^3 and 12.27 Å^3, respectively. The expanded atomic volume of the AFM phases of tetragonal Fe stands in marked contrast to the magnetovolume effect observed in cubic Fe (both bcc and fcc) where the FM phase always has a larger atomic volume than the AFM state.[56]

Comparing these values with the data from Table IV obtained for the thickest film, 4-ML Fe/Rh(100) in the FM state, i.e., $c/a=0.85$ and an average magnetic moment $m=2.67\mu_B$ we infer that the film is in expanded state. This can be ascribed to enhanced surface and interface magnetic moments which are responsible for the larger c/a ratio (cf. Fig. 1). A similar conclusion holds for a 3-ML film in the FM phase. In the layered AFM 3-ML film ($udu|$Rh), the average axial ratio is expanded to $c/a=0.89$, in analogy with the epitaxially constrained bulk phase.

There has been some discussion in the literature about the appropriate description of the film structure. For a fct phase c/a should be close to 1, whereas for bct phase c/a is close to 0.7. The axial ratio $c/a=0.85$ obtained for FM 4-ML film lies precisely in-between these two limits, so that the bct and fct structures cannot be distinguished from the geometric point of view. In the case of nonmagnetic films with $c/a=0.82$ the characterization as a bct structure seems to be slightly more appropriate.

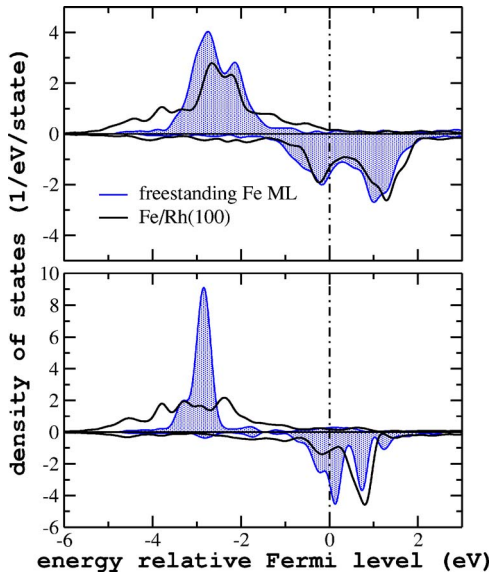

FIG. 2. (Color online) Comparison of spin-polarized local electronic density of states of a free-standing Fe monolayer matching the structure of the Rh(100) surface with a 1-ML Fe/Rh(100) film in (top panel) FM and (bottom panel) AFM state.

C. Origin of antiferromagnetism in Fe/Rh(100) monolayers

The surprising antiferromagnetism of Fe monolayers on Rh(100) still requires some explanation. To find an answer, we have calculated the total energy of freestanding Fe monolayer matching the structure of the Rh(100) surface in the FM and AFM phases. We find that the FM solution is lower in energy by 297 meV/Fe atom, the magnetic moment in both phases is $|m|=3.10\mu_B$. This means that the antiferromagnetic ground state of 1-ML Fe/Rh(100) cannot be attributed to the reduced dimensionality of the ML, but must be due to the hybridization of the Fe orbitals with the substrate. Figure 2 shows the spin-polarized density of states (DOS's) for the freestanding and adsorbed monolayers. For the FM freestanding ML we find a fully occupied majority *d* band and a minority *d* band with a pronounced bonding/antibonding splitting, with the Fermi level just below the DOS minimum, whereas the AFM phase is characterized by narrower *d* bands and a position of the Fermi level close to a DOS maximum in the minority band, disfavoring the AFM phase. The *d* bands of the Rh-supported Fe monolayer are strongly broadened by hybridization with the Rh *d* band across the interface. The broadening affects the AFM phase more than the FM phase and results in a shift of *d* states to higher binding energies stabilizing the FM phase.

This is not the first case where the hybridization of the electronic eigenstates of the magnetic adlayer with those of the substrate changes the magnetic ground state of the monolayer compared to that of the bulk. Earlier DFT studies[57,58] have predicted AFM ordering in Fe/W(100) and Co/W(110), and very recently DFT calculations found FM ordering on Mn/W(100) monolayers.[59,60] In all cases adlayer-substrate hybridization has been identified as responsible for driving the monolayer into a magnetic ground state different from that of the bulk metal.

TABLE V. Adsorption energy E_{ad}, intramolecular ($\omega_{C\text{-}O}$) and molecule-substrate ($\omega_{S\text{-}CO}$) stretching frequencies, molecular bond length $d_{C\text{-}O}$, carbon-metal distance $d_{C\text{-}Rh}$, and adsorption-induced change of the interlayer distance of the surface layer $\Delta\bar{d}$ for 0.5 and 1 ML of CO on Rh(100).

	E_{ad} (eV)	$\omega_{C\text{-}O}$ (cm^{-1})	$\omega_{S\text{-}CO}$ (cm^{-1})	$d_{C\text{-}O}$ (Å)	$d_{C\text{-}Rh}$ (Å)	$\Delta\bar{d}$ (Å)
$\theta=0.5$						
top	1.57	2026	441	1.168	1.864	0.070
bridge	1.56	1898	349	1.182	2.049	0.061
hollow	1.37	1732	231	1.203	2.263	0.082
$\theta=1.0$						
top	0.90	2083	426	1.165	1.864	0.133
bridge	1.15	1993	373	1.175	2.045	0.211
hollow	0.69	1855	261	1.190	2.249	0.154

IV. CO ADSORPTION

By comparing the adsorption properties of CO on Fe/Rh(100) films with those on clean fcc Rh(100), bcc Fe(100) surfaces and on near-fcc Fe/Cu(100) films we can achieve a further characterization of the strained Fe films on a Rh substrate. HREELS experiments[36] on CO adsorbed on Fe/Rh(100) reported three stretch bands attributed to atop, bridge, and hollow bonding sites for CO molecule. For CO on Rh(100) surfaces, infrared adsorption spectroscopy[61,62] (IRAS) identified two coverage-dependent vibrational bands assigned to top and bridge-adsorbed CO, in agreement with DFT studies.[63] For CO adsorbed on the open (100) surface of bcc Fe a particularly soft C-O stretching mode signals a tilted adsorption geometry in a fourfold hollow[13,16] (see the more detailed discussion in the Introduction), whereas on the more close-packed bcc Fe(110) surface[64] and on Fe/Cu(100) films[19,20] only upright adsorption geometries on top and bridge sites have been reported. DFT studies are in good agreement with the experimental findings.[17,21,65]

A. CO adsorption on Rh(100)

In order to asses the effect of a capping Fe layer on the adsorption characteristics of CO molecules, we have also considered CO on a bare Rh(100) surface. CO adsorption on this surface has been theoretically explored in the past by several authors.[44,63,66] However, these studies were performed for thinner slabs, smaller energy cutoff parameter and sometimes with different exchange-correlation functionals. For this reason as well as for the sake of internal consistency of our results, we prefer to recompute the adsorption energies and vibrational frequencies for the highly symmetric atop, bridge and hollow positions (a tilted adsorption geometry in the hollow was found to be unstable). The results for half and full ML coverage are summarized in Table V. The adsorption energies have been calculated according to the expression

$$E_{ad} = (N_{CO}E_{CO} + E_{subs} - E_{CO+subs})/N_{CO}, \quad (1)$$

where E_{CO} is the energy of the isolated CO molecule, E_{subs} is the total energy of the clean substrate, $E_{CO+subs}$ is the total

TABLE VI. Calculated adsorption properties of CO on 1-ML Fe/Rh(100) films at $\theta=0.5$ ML coverage: adsorption energy E_{ad} (in eV per molecule), magnetic moments of Fe atoms binding a CO molecule (m_{ad}) or left vacant (m_{free}), frequencies of intramolecular stretching modes ($\omega_{C\text{-}O}$) and adsorbate-substrate stretching vibrations $\omega_{S\text{-}CO}$, molecular bond-length $d_{C\text{-}O}$, and metal-carbon distance $d_{C\text{-}Fe}$, average adsorbate-induced change of Fe-Fe interlayer distances, $\Delta\bar{d}=\bar{d}[\mathrm{CO+Fe/Rh(100)}]-\bar{d}[\mathrm{Fe/Rh(100)}]$, total change of magnetization Δm, and tilting angle of the C-O bond with respect to the surface normal φ (where applicable).

	E_{ad} (eV)	m_{ad} (μ_B)	m_{free} (μ_B)	$\omega_{C\text{-}O}$ (cm^{-1})	$\omega_{S\text{-}CO}$ (cm^{-1})	$d_{C\text{-}O}$ (Å)	$d_{C\text{-}Fe}$ (Å)	$\Delta\bar{d}$ (Å)	Δm (μ_B)	φ (deg)
AFM, $\theta=0.5$										
top	1.43	−1.94	3.14	1969	380	1.174	1.800	0.035	−0.60	0.0
bridge	1.10	−2.54	2.54	1858	312	1.188	1.995	0.044	0.00	0.0
hollow	0.93	−2.56	2.56	1615	218	1.222	2.200	0.087	0.00	0.0
t hollow	0.87	−2.46	2.49	1502	305	1.245	2.006	0.077	−0.01	36.9
FM, $\theta=0.5$										
top	1.37	2.13	3.17	1951	351	1.176	1.814	0.028	−0.76	0.0
bridge	1.19	2.53	2.53	1841	326	1.191	1.960	0.023	−0.51	0.0
hollow	1.25	2.66	2.66	1593	207	1.226	2.173	0.031	−0.74	0.0
t hollow	1.23	2.57	2.65	1517	303	1.242	2.066	0.023	−0.85	26.8
NM, $\theta=0.5$										
top	2.01	0.00	0.00	1985	425	1.173	1.779	0.026	0.00	0.0
bridge	1.97	0.00	0.00	1860	372	1.189	1.938	0.045	0.00	0.0
hollow	1.64	0.00	0.00	1559	180	1.230	2.131	0.136	0.00	0.0
t hollow	2.10	0.00	0.00	1241	452	1.308	1.903	0.174	0.00	56.9

energy of the slab with CO molecules on the surface, and N_{CO} is the number of CO molecules per surface cell.

At a half-monolayer coverage the top (*t*) and bridge (*b*) sites have almost the same adsorption energies, in agreement with a mixed occupation of both sites as deduced from the IRAS experiments. At a coverage of $\theta=1$ ML the bridge sites are clearly favored, but the integrated adsorption energies are strongly decreased in comparison to a lower saturation coverage. The calculated CO adsorption energy (including zero-point energy corrections) is 132 kJ/mol at a half-monolayer coverage, this is slightly larger than the experimental value of 110 kJ/mol deduced from the coverage-corrected leading-edge analysis.[66] The lower adsorption energy obtained using the RPBE functional represents an improvement compared to 202 kJ/mol predicted using the PW91 functional.[63] More importantly, the RPBE functional also leads to a different result for the site preference: whereas the calculations using the PW91 functional predict the bridge site to be strongly preferred already at half-monolayer coverage (with an energy difference of 0.13 eV and 0.14 eV relative to the hollow and top sites respectively), the RPBE calculations disfavor the hollow site—again this improves agreement with experiment. On the other hand, adsorption geometries and stretching frequencies are hardly affected by the change of the functionals. Our calculated C-O stretching frequencies of 2026 cm^{-1} (*t*) and 1898 cm^{-1} (*b*) are in good agreement with the experimental values of 2035 to 2052 cm^{-1} (*t*) and 1895 to 1915 cm^{-1} (*b*) from the IRAS experiments.[61,62]

B. CO adsorption on 1-ML Fe/Rh(100) films

All the parameters data describing the adsorption of CO on a 1-ML Fe/Rh(100) film are summarized in Tables VI and VII for the coverage $\theta=0.5$ and $\theta=1$, respectively. Adsorption tends to locally demagnetize the substrate, in the Table VI m_{ad} stands for the magnetic moment of a surface atom binding to the adsorbed molecule, whereas m_{free} denotes the local magnetic moment on a free surface atom, Δm stands for the adsorbate-induced change in the net magnetization of the adlayer. The intramolecular C-O stretching frequencies $\omega_{C\text{-}O}$ and the adsorbate-substrate stretching frequencies $\omega_{S\text{-}C}$ have been calculated via a diagonalization of the local dynamical matrix. The adsorption induces a slight outward relaxation of the top layers measured by $\Delta\bar{d}$, defined as

$$\Delta\bar{d}=\bar{d}_{CO+subs}-\bar{d}, \tag{2}$$

where $\bar{d}$ is the average interlayer distance in Fe/Rh(100) films tabulated in Tables I–IV. For the adsorption in a hollow, where we have found also (meta)stable titled geometries, the tilt angle φ of CO molecule relative to the surface normal is given. In the course of the structural optimization no preferential tilt plane was assumed, therefore the resultant geometries stand for the locally most stable solutions. In all configurations with an inclined CO molecule the O atom is located near a bridge site (see Fig. 3), forming two equivalent bonds with Fe atoms.

1. Site preference and adsorption energies

Our results display a strong dependence of the adsorption properties on coverage and on the magnetic state of the substrate. As seen from Table VI, at half-monolayer coverage the highest adsorption energy is predicted for a tilted CO

TABLE VII. Calculated adsorption properties of CO on 1-ML Fe/Rh(100) films at θ=1.0 ML coverage, cf. Table VI.

	E_{ad} (eV)	m (μ_B)	$\omega_{C\text{-}O}$ (cm^{-1})	$\omega_{S\text{-}CO}$ (cm^{-1})	$d_{C\text{-}O}$ (Å)	$d_{C\text{-}Fe}$ (Å)	$\Delta\bar{d}$ (Å)	Δm (μ_B)
AFM, θ=1.0								
top	1.38	±2.04	1972	332	1.164	1.820	0.053	0.00
bridge	1.43	±2.04	1903	314	1.176	2.027	0.075	0.00
hollow	0.85	±1.87	1690	249	1.206	2.152	0.221	0.00
FM, θ=1.0								
top	0.68	1.79	2068	387	1.165	1.811	0.000	−1.25
bridge	0.72	2.04	1966	296	1.175	2.031	0.034	−0.99
hollow	0.57	2.03	1728	230	1.211	2.128	0.093	−1.01
NM, θ=1.0								
top	1.38	0.00	2074	422	1.165	1.788	0.067	0.00
bridge	1.42	0.00	1973	353	1.176	2.003	0.105	0.00
hollow	1.02	0.00	1732	212	1.207	2.133	0.279	0.00

placed in a hollow site on a nonmagnetic film. This configuration, depicted in detail in Fig. 3, is distinguished by an extremely low vibrational frequency of 1241 cm^{-1} and a C-O bond stretched by 0.1 Å relative to the gas phase. In this respect our findings are similar to the results of Sorescu *et al.*[17] and of Stibor *et al.*[65] for CO adsorption on a FM bcc Fe(100) surface and to the experiments[14–16] mentioned in the Introduction. This close similarity is a bit surprising since the contrasting adsorption behavior of CO on Fe(100) and Fe(110) has been attributed to the low density of the bcc (100) surface, while the in-plane lattice spacing of the Fe/Rh(100) overlayer is contracted by about 5% compared to the interatomic distances in an Fe(100) plane.

For the stable AFM ground state of Fe/Rh(100) and in the FM state, the adsorption energy is strongly reduced and adsorption on top of an Fe atom is strongly preferred. The reduced adsorption energy is a direct consequence of the exchange splitting [which is nearly 3 eV in the Fe/Rh(100) film] reducing the contribution of the majority-spin electrons to the formation of the adsorbate-substrate bond. However, the difference in the adsorption energies of 670 meV/molecule (top/AFM vs tilted-hollow/NM) is not enough to overcompensate the magnetic energy difference of 820 meV/Fe atom calculated for the clean surface, the difference in the total energies is 503 meV/Fe atom in favor of top-adsorbed CO on AFM Fe/Rh(100). However, one has to remember the magnetic energy differences of only 28 meV/Fe atom (AFM vs FM) and 820 meV/Fe atom (AFM vs NM). The former shows that the AFM ordering temperature will be rather low, the latter value suggests that the state stable above the ordering temperature will be rather a disordered local moment state than a truly nonmagnetic state.

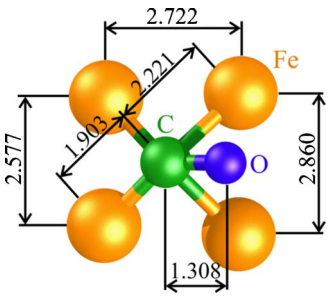

FIG. 3. (Color online) Local geometry of the CO adsorbed on a NM Fe/Rh(100) overlayer in a tilted position. All distances are given in Å units.

At full monolayer coverage (see Table VII), adsorption energies are strongly reduced for NM or FM Fe layers, while only a modest reduction is calculated for the AFM state. In both the AFM and NM phases, bridge site is now preferred, with almost equal adsorption energies. Top-site adsorption is disfavored only by 50 meV/molecule.

2. Structure and magnetism of substrate

CO adsorption induces an outward relaxation of the surface layer, and a local demagnetization of the Fe atoms bound to the adsorbate. The outward relaxation is strongest for adsorption in the hollow and increases with coverage. This effect is related to a more pronounced back donation from the d band of the substrate to the antibonding $2\pi^*$ orbital (as demonstrated by a stronger increase of the C-O bond length), which leads to a weakening of the Fe-Rh back bonds. In magnetically polarized films the majority-spin d band is shifted to higher binding energies (cf. Fig. 4) so that they cease to participate in the charge transfer process and the outward relaxation is correspondingly less pronounced. As expected, the outward relaxation increases with coverage.

Moreover, for atop adsorption at θ=0.5 only half of the Fe atoms are in direct contact with a CO molecule, whereas the other half is exposed to vacuum. The magnetic moment of the substrate atoms binding to the adsorbate is strongly reduced, while on the clean surface site, the moment is even slightly enhanced. This asymmetry gives rise to a buckling of the top layer by 0.03 Å in the stable AFM state, by 0.09 Å in the FM state, but by only 0.02 Å in the NM state (Fe atom

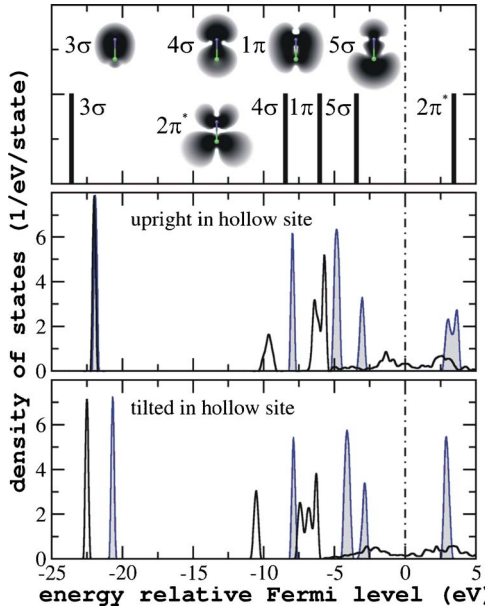

FIG. 4. (Color online) Top panel: energy levels of a free CO molecule. The insets in the figure show the spatial electron distribution of the molecular 3σ, 4σ, 1π, 5σ, and $2\pi^*$ orbitals. Middle and low panels: The density of states projected on a CO molecule adsorbed on a nonmagnetic Fe/Rh(100) overlayer (coverage 0.5 ML CO) in either an upright hollow position (middle panel) or in a tilted state (bottom panel). The shaded curves represent the density of states obtained for the CO molecules in the same geometry as above, just with removed support, i.e., for freestanding CO layers.

near CO is pulled upwards). For bridge and hollow-adsorbed CO all surface Fe atoms bind to the adsorbate. In this case all magnetic moments are homogeneously reduced by about $0.5\mu_B$ and there is no buckling of the surface layer. However, CO adsorbed in a hollow site binds also to the Fe atoms in the subsurface layer, inducing a buckling of the subsurface layer by about 0.1 Å, independent of the magnetic state of the substrate. A tilted adsorption geometry breaks the fourfold symmetry of the adsorption configuration and leads to a small difference in the magnetic moments.

Due to the local demagnetization of the Fe layer by top-adsorbed CO, for half-monolayer coverage the AFM phase is transformed into a ferrimagnetic configuration with a net magnetization of $0.6\mu_B$ per surface atom. For full monolayer coverage the demagnetization is even more pronounced ($\Delta m \sim 1\mu_B$), but as all surface atoms bind to the adsorbate, the net magnetization of the surface remains zero. We note that a moderate moment on Rh atoms close to Fe atoms develops, which is oriented parallel to Fe moments and has a size of at most $0.32\mu_B$ ($\theta=1$, FM films, hollow site).

Due to the interaction with a spin-polarized substrate, the adsorbed CO molecule acquires a small magnetic moment oriented antiparallel to the substrate moment. The magnitude of the induced moment depends on the coordination of the adsorption site. We calculate moments of $-0.22/-0.17/-0.08\mu_B$ for CO in $h/b/t$ sites, which are independent of an eventual tilt angle.

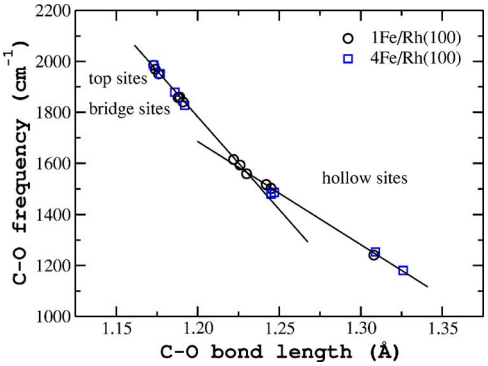

FIG. 5. (Color online) Correlation between the C-O bond length and the C-O stretching frequency. The points were obtained for the 0.5 ML coverage of CO molecules adsorbed on 1Fe/Rh(100) and 4Fe/Rh(100) films. All investigated magnetic states are taken into account.

3. Vibrational frequencies

The calculated frequencies of the stretching modes of the intramolecular C-O bond and the adsorbate-substrate bond are listed in Table VI for a CO coverage of $\theta=0.5$ and in Table VII for $\theta=1$. It is well known from many studies on CO chemisorption on transition metals (see, e.g. Gajdoš *et al.*[39]) that the red shift of the C-O stretching frequency increases in proportion to the coordination number, and that there is a tight correlation between the softening of the stretching mode and the elongation of the molecular bond length. For $\theta=0.5$ this correlation is displayed in Fig. 5. Interestingly, the correlation is independent of the particular magnetic state and the thickness of the Fe layer, but it depends on the adsorption geometry. Figure 5 shows two regions with linear bond-length-frequency correlation, a first one with a steeper slope for upright CO, and a second one with smaller slope for CO adsorbed in a tilted configuration in a hollow. The anomalously soft stretching frequencies for a tilted adsorption geometry in the fourfold hollow of about 1500 cm^{-1} (metastable configuration in the AFM and FM phases) and 1200 cm^{-1} (stable configuration in the NM state) represent a fingerprint of the adsorption geometry. The two regions in the bond-length-frequency correlation reflect distinctly different mechanisms of CO bonding in an upright and in a tilted configuration. Such a tight correlation is not found for the full coverage, probably because of increased lateral interactions, but the trend is still roughly followed. At full coverage the redshift of the C-O stretching modes is reduced, as expected from the smaller adsorption energy.

4. Comparison with experiment

The very soft stretching mode of 1210 cm^{-1} for CO adsorbed on bcc α-Fe(100) is a clear signal for the bcc-like character of the substrate. However, for CO adsorbed on 1-ML Fe/Rh(100), comparison of our results with experimental data[36] is hampered by the lack of information on the surface coverage and the magnetic state of Fe overlayer. The HREEL spectra were taken at 100 K with a high CO partial pressure of 15 L. According to our results compiled in Tables VI and VII, the measured HREELS loss peaks at 2060, 1950,

1630 cm^{-1} can be assigned to CO adsorbed upright in top, bridge, and hollow sites at coverages intermediate between $\theta=0.5$ and $\theta=1$. For the two high-frequency modes, agreement with experiment is best for a nonmagnetic Fe layer. Annealing to 280 K eliminates both the 2060 cm^{-1} and 1630 cm^{-1} features, in agreement with the fact that at saturation the highest adsorption energy is calculated for bridge-adsorbed CO. The HREEL spectra contain a broad peak centered around 350 cm^{-1} in rough agreement with our calculated adsorbate/substrate stretching modes. However, as vibrations in this range couple with phonon modes of the substrate, a quantitative comparison of theory and experiment is not meaningful.

Hence we are led to two conclusions: (i) Even at the low temperatures of the HREELS experiment, the 1-ML Fe/Rh(100) are probably not in a magnetically ordered state. However, the large energy difference between the NM and either magnetically ordered phases combined with the small energy difference in the AFM and FM configurations suggests that the film is in a disordered local moment state. (ii) Any feature indicating a tilted CO adsorption geometry in analogy to bcc Fe(100) is missing. However, this could be a consequence of strong repulsive lateral interactions at high coverage and does not exclude that a tilted configuration might be stable at lower coverage.

5. CO tilting

The mechanism leading to a tilted adsorption geometry for CO is still not completely understood. Conventionally, the mechanism for the adsorption of CO on transition metal surfaces is discussed in terms of the Blyholder model.[39,67] The molecular eigenstates of CO interacting with the substrate are the 4σ, 5σ, 1π, and $2\pi^\star$ orbitals (see Fig. 4). For gas-phase CO, the charge density in the 4σ state is concentrated around the O atom, upon adsorption charge is depleted around the O atom and accumulated in the region between the C atom and the substrate. In the 5σ state, charge is initially concentrated at the C atom, upon adsorption it flows to the O atom, into the C-O bonding region, and, most importantly, to the substrate. This charge transfer leads to the formation of a lone pair on the oxygen site, as observed experimentally by Nilsson *et al.*[68] The 1π and $2\pi^\star$ orbitals interact with the d_π manifold of the substrate. This leads to a broadening of the 1π states, but only a modest charge transfer from 1π states located around the O atom into the metal-carbon bonding region. More important is the back donation from the d_π states of the metal to the antibonding $2\pi^\star$ states, leading to the stretching of the C-O bond. The amount of back donation is important as it determines also the redshift of the C-O stretching mode.

In an upright adsorption geometry in the fourfold hollow, both p_π orbitals interact symmetrically with the $d_{t_{2g}}$ states located on all four of the surrounding substrate atoms, as visualized by the charge-flow diagram of Fig. 6. The dominant effect is the depletion of the 5σ state by donation to the substrate and the incipient population of the antibonding $2\pi^\star$ state by back donation. In the projected DOS seen in Fig. 4, the adsorbate/substrate interaction is reflected by a strong broadening of the $2\pi^\star$ states, and a shift of the 5σ, 1π, and 4σ states to higher binding energies. In an adsorption geometry where the CO molecule is tilted towards a neighboring bridge site, the fourfold symmetry is broken and the charge-flow diagram shows an increased back-donation into the $2\pi^\star$ states (whose charge distribution now overlaps with bond charge of the Fe-C bonds) and in addition a pronounced charge redistribution around the O atom. O p_σ states are depleted, charge is transfered into asymmetrically polarized

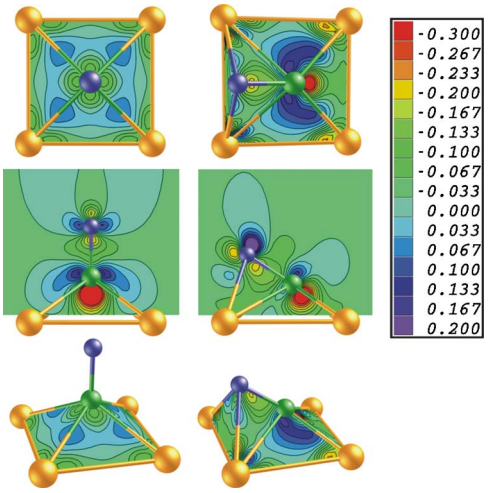

FIG. 6. (Color online) Charge-flow distribution in the form of isocontour plots for CO adsorbed in a fourfold hollow of nonmagnetic Fe/Rh(100) in an upright (on left) and tilted (on right) configuration. From bottom to top: perspective view of the charge flow on the facets of the flat Fe-C pyramid (upright geometry) and on the Fe-C-O tetrahedron (tilted geometry); middle row: charge flow in the CO tilt plane; top row: looking down on the CO-Fe adsorbate-substrate complex. The units in the legend table are electron/$Å^3$.

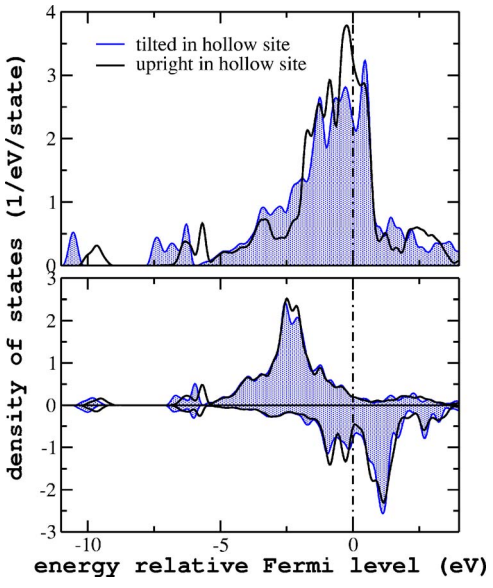

FIG. 7. (Color online) Electronic density of states in the Fe layer of a 1-ML CO/Fe/Rh(100) film (CO coverage 0.5 ML) in a nonmagnetic (top panel) and in a ferromagnetic state (lower panel), as calculated for CO in a fourfold hollow in upright and in tilted configurations.

TABLE VIII. Calculated adsorption properties of CO on 4-ML Fe/Rh(100) films at θ=0.5 ML coverage, for the nomenclature cf. Table VI.

	E_{ad} (eV)	m_{ad} (μ_B)	m_{free} (μ_B)	$\omega_{\text{C-O}}$ (cm^{-1})	$\omega_{\text{S-CO}}$ (cm^{-1})	$d_{\text{C-O}}$ (Å)	$d_{\text{C-Fe}}$ (Å)	$\Delta\bar{d}$ (Å)	Δm (μ_B)	φ (deg)
FM, θ=0.5										
top	1.21	1.84	3.09	1951	390	1.177	1.811	0.002	−0.44	0.0
bridge	1.01	2.41	2.41	1828	291	1.192	1.979	0.000	−0.52	0.0
hollow	1.09	2.38	2.38	1486	243	1.247	2.095	0.011	−0.51	0.0
t hollow	1.48	2.22	2.36	1253	460	1.309	1.957	−0.008	−0.72	48.0
NM, θ=0.5										
top	1.89	0.00	0.00	1986	415	1.173	1.789	0.005	0.00	0.0
bridge	1.91	0.00	0.00	1879	352	1.186	1.957	−0.003	0.00	0.0
hollow	1.52	0.00	0.00	1481	204	1.245	2.074	0.025	0.00	0.0
t hollow	2.06	0.00	0.00	1181	447	1.326	1.939	0.023	0.00	50.1

O p_π states. We also observe the formation of a weak Fe *d* and O *p* bond. The local DOS on the molecule shows that this leads to a further broadening of the 1π and $2\pi^\star$ states and an increased occupation of the latter (which in turn causes a weakening of the intramolecular bond). Even the low-lying 3σ states are affected by the tilting, but the upshift due to lateral dipole-dipole interaction is compensated by a downshift caused by the interaction with the substrate. The tilting is energetically favorable only if the gain in adsorbate/substrate bonding energy overcompensates the lateral repulsion which increases from 0.31 eV/molecule to 0.98 eV/molecule as the tilt angle increases from zero to φ=56.9°. On the (100) surface of FM Fe, the CO interacts mainly with the minority Fe *d* band, the majority *d* band being pushed below the Fermi level.[65] The DOS of the out of plane $d_{t_{2g}}$ states has a pronounced peak at the Fermi level. Tilting of the molecule leads to an interaction of one of these orbitals with an O *p* orbital and to a shift of the corresponding Fe *d* states to higher binding energies. For 1-ML Fe/Rh(100) the situation is quite different as presented in Fig. 7. For a FM or AFM film, the Fermi level falls close to a minimum in the *d* band DOS, and a tilted configuration is only metastable. Figure 7 displays only minimal variation of the *d* band DOS between the upright and tilted configurations. For a NM film, the DOS has a pronounced peak very close to E_F if CO is adsorbed in an upright position. Tilting of the molecule leads to a broadening of the Fe *d* band, formation of a local DOS minimum at E_F and a shift of $pd\pi$ bonding states to lower energy stabilizing this configuration.

C. CO adsorption on thicker Fe/Rh(100) films

In this section we shall focus on the chemisorptive properties of CO molecules on 4-ML thick Fe/Rh(100) films, our results are summarized in Tables VIII and IX. We find a strong dependence of the stable adsorption geometries on coverage and on the magnetic state of the film. At half-monolayer coverage, adsorption in a fourfold hollow in strongly tilted configurations is preferred over adsorption at top or bridge sites, while an upright CO molecule in the hollow is a much less favorable geometry. The difference in the adsorption energies for NM and FM substrates is 0.58 eV/molecule, but this is evidently not sufficient to overturn the magnetic energy gain by the onset of ferromagnetism.

As the coverage is increased to a full CO monolayer, the site preference remains for the hollow (but now only an upright configuration is stable) on the FM film, while on a NM

TABLE IX. Calculated adsorption properties of CO on 4-ML Fe/Rh(100) films at θ=1.0 ML coverage, for the nomenclature cf. Table VI.

	E_{ad} (eV)	m (μ_B)	$\omega_{\text{C-O}}$ (cm^{-1})	$\omega_{\text{S-CO}}$ (cm^{-1})	$d_{\text{C-O}}$ (Å)	$d_{\text{C-Fe}}$ (Å)	$\Delta\bar{d}$ (Å)	Δm (μ_B)
FM, θ=1.0								
top	0.55	−0.18	2073	400	1.165	1.792	0.036	−3.24
bridge	0.57	−0.86	1977	340	1.175	2.011	0.019	−3.97
hollow	0.70	1.68	1704	259	1.216	2.103	−0.007	−1.10
NM, θ=1.0								
top	1.32	0.00	2075	415	1.165	1.800	−0.005	0.00
bridge	1.31	0.00	1978	348	1.175	2.013	−0.011	0.00
hollow	0.92	0.00	1693	219	1.214	2.102	−0.059	0.00

film top and bridge site (which are energetically almost degenerate) are favored over the hollow site. At this high coverage the demagnetizing influence of the molecular adlayer is particularly pronounced. If CO is adsorbed in the hollow, the magnetic moments of the Fe atoms in the surface layer are reduced to about half their magnitude on the clean surface, for CO on top or bridge sites, the surface layer is even completely demagnetized, with only small antiparallel moments on the Fe atoms. A similar adsorbate-induced transformation of the magnetic structure has been found previously on CO-covered Fe/Cu(100) films.[21]

The vibrational eigenmodes are almost unchanged relative to the Fe/Rh(100) monolayer. Experimentally, Egawa *et al.*[36] have reported that the high-frequency HREELS peaks measured at saturation merge into a single peak at 2000 cm^{-1} as the thickness of the Fe film increases to 4 ML—this is in agreement with a mixed population of top and bridge sites as suggested by the closeness of the adsorption energies. Again a weaker, rather broad feature at 1630 cm^{-1} which disappears after annealing at 280 K is reported. This can again be assigned to hollow-adsorbed CO. Due to the high partial pressure of CO used in the experiments, the lower-coverage regions are not probed by the experiment.

An interesting conjecture is that as the system goes through the magnetic ordering transition, site preference changes from hollow in the FM state to mixed top/bridge in the NM site, accompanied by a strong increase of the adsorption energy. Evidently it would be interesting to observe this reversal of the site preference. However, it has also be kept in mind that above the Curie temperature (which is unknown) the system will assume a disordered local moment state.

V. CONCLUSIONS

We have presented a detailed *ab initio* investigation of the structural, magnetic, and chemical properties of Fe films grown on Rh(100) substrates. Our results confirm that Fe/Rh(100) films are indeed a very interesting model system for investigating the properties of tetragonal Fe at an axial ratio intermediate between the bcc and fcc structures. The tetragonal axial ratio calculated from the average of the relaxed interlayer distances is $c/a \sim 0.85$, i.e., just halfway between the bcc and fcc limits. This corresponds to a slightly expanded volume per Fe atom of about 12.3 $Å^3$ compared to bulk Fe. The magnetic ground state of films with a thickness above 1 ML is ferromagnetic, with an average magnetic moment of $2.7-2.8\mu_B$, i.e., enhanced compared to bulk FM bcc Fe due to the expanded volume and the usual surface-induced enhancement.

However, the magnetic properties of the tetragonal Fe films are quite different from both bcc α-Fe and fcc γ-Fe. In α-Fe the magnetic energy difference between the FM and AFM phases is about half as large as the FM-NM energy difference [$\Delta E(NM-FM)=550$ meV/atom, $\Delta E(AFM-FM)=210$ meV/atom].[56] In γ-Fe, magnetic energy differences are significantly reduced [$\Delta E(NM-FM)=40$ meV/atom, $\Delta E(AFM-FM)=-24$ meV/atom].[4,56] In Fe/Rh(100) films, the energy difference stabilizing the FM state is large [$\Delta E(NM-FM)\sim 500$ meV/atom] as in α-Fe, but that between the AFM and FM phases is much smaller [$\Delta E(AFM-FM)\sim 100$ meV/atom]. In addition, we have found metastable ferrimagnetic phases at energies intermediate between the FM and AFM configurations. This provides evidence for the existence of strong competing ferromagnetic and antiferromagnetic exchange interactions, as expected for a tetragonal structure intermediate between the FM bcc and the AFM fcc phases. The existence of competing interactions also explains the observation of a strong reduction of the magnetic ordering temperature with decreasing films thickness[28,29] and further suggests that above the ordering temperature the films will assume a disordered local moment state.

For monolayer Fe/Rh(100) our calculations show that the strong Fe *d*-Rh *d* hybridization at the interface leads to an AFM ordering of the film. This finding is in line with earlier predictions of AFM in Fe/W(100) and Co/W(110) monolayers, and of FM in Mn/W(100) monolayers, in all cases the interaction with substrate reverses the magnetic ordering in the adlayer relative to the bulk material.[57–60] However, the smallness of the AFM-FM energy difference suggests a low antiferromagnetic ordering temperature and again a disordered local moment state at ambient temperatures.

Our studies of CO adsorption on Fe/Rh(100) reveal a strong dependence on coverage and on the magnetic state of the films. The adsorption energies calculated for magnetically ordered films are always significantly lower than for nonmagnetic films. This is a consequence of the complete occupation of the majority-spin band which allows only the minority electrons to interact with the adsorbate states. In addition, magnetic ordering can change the preferred adsorption geometry. For 0.5 ML CO on 1-ML Fe/Rh(100) films, linear on-top adsorption is preferred in the magnetically ordered AFM phase, while on a nonmagnetic film CO assumes a tilted configuration in a fourfold hollow, in analogy to CO-adsorption on bcc Fe(100). If the coverage is increased to a full monolayer, nearly equal adsorption energies are calculated for top and bridge sites, with no tilting. The experimental adsorption studies of Egawa *et al.*[36] have been performed at exposures of 15 L CO, i.e., at saturation (although the saturation limit is unknown). Assuming a saturation coverage of about 0.7 ML CO and an essentially linear variation of the adsorption energies with coverage, our results are compatible with the observation that at low temperatures CO forms a disordered overlayer with nearly equal occupation probabilities for top and bridge sites, and a small fraction of CO in upright hollow sites. Our calculated CO stretching frequencies are in good agreement with the HREELS experiments. Our prediction that at low coverages a tilted adsorption geometry in the fourfold hollow with a CO stretching mode of about 1240 cm^{-1} is stabilized is confirmed by the observation of a 1200 cm^{-1} loss features at incipient adsorption.[36]

Results for CO on a 4-ML Fe/Rh(100) film are closer to those for adsorption on bulk bcc Fe(100): at 0.5-ML coverage, a tilted adsorption geometry in a fourfold hollow is strongly preferred, in the ferromagnetic as well as in the nonmagnetic state. At full ML coverage, the lateral interactions suppress any tilting. In this case, the site preference changes from hollow to top or bridge as the films undergoes

a ferromagnetic to paramagnetic transition. Again our results are compatible with the experimental observations on saturated CO/Fe/Rh(100), but evidently it would be of great interest to study adsorption at lower coverages.

A remarkable result is the strong local demagnetizing influence of the adsorbate. Magnetic moments of Fe atoms bonding to the adsorbed CO are strongly reduced, while those on "clean" Fe sites remain nearly unaffected. Interestingly, the demagnetizing effect is stronger for the FM 4-ML Fe films than for the AFM 1-ML film. At full 1-ML CO coverage, the top Fe layer is completely demagnetized (or develops even a small antiparallel moment), while a substantial FM moment is conserved if the molecule is adsorbed in a hollow. These observations parallel earlier results for CO on bcc Fe(100).[65]

In summary, our results show that the magnetic properties of tetragonal Fe/Rh(100) are determined by competing ferromagnetic and antiferromagnetic interactions. This leads to a reduced magnetic ordering temperature and a tendency to a disordered local moment state. Our studies of CO adsorption suggest that the chemical properties of these films are closer to those of α-Fe than of γ-Fe surfaces. Monolayer Fe/Rh(100) films are found to be antiferromagnetic, but this antiferromagnetism is not a structural effect expressing a similarity with fcc γ-Fe, but is substrate induced. Interestingly, the adsorption properties of the nonmagnetic monolayers are close to those of bcc Fe(100) surfaces, with a stable tilted adsorption geometry. We hope that our results will stimulate adsorption experiments at low CO coverages.

ACKNOWLEDGMENT

We gratefully acknowledge support by the Austrian Science Funds (FWF) under Project No. 16184-N02.

*Electronic address: Daniel.Spisak@univie.ac.at

[1] See, e.g., J. Shen and J. Kirschner, Surf. Sci. **500**, 300 (2002); and further references given therein.
[2] A. Logadottir, T. H. Rod, J. K. Nørskov, B. Hammer, S. Dahl, and C. J. H. Jacobsen, J. Catal. **197**, 229 (2001).
[3] Y. Tsunoda, N. Kunitomi, and R. M. Nickow, J. Phys. F: Met. Phys. **18**, 1405 (1987); **18**, 1421 (1987).
[4] M. Marsman and J. Hafner, Phys. Rev. B **66**, 224409 (2002).
[5] J. R. Dutcher, B. Heinrich, J. F. Cochran, D. A. Steigerwald, and W. F. Egelhoff, Jr., J. Appl. Phys. **63**, 3464 (1988).
[6] J. Thomassen, F. May, B. Feldmann, M. Wuttig, and H. Ibach, Phys. Rev. Lett. **69**, 3831 (1992).
[7] S. Müller, P. Bayer, C. Reischl, K. Heinz, B. Feldmann, H. Zillgen, and M. Wuttig, Phys. Rev. Lett. **74**, 765 (1995).
[8] A. Biedermann, M. Schmid, and P. Varga, Phys. Rev. Lett. **86**, 464 (2001).
[9] D. Spišák and J. Hafner, Phys. Rev. B **61**, 16 129 (2000).
[10] D. Spišák and J. Hafner, Phys. Rev. Lett. **88**, 056101 (2002).
[11] T. Bernhard, M. Baron, M. Gruyters, and H. Winter, Phys. Rev. Lett. **95**, 087601 (2005).
[12] D. W. Moon, D. J. Dwyer, and S. L. Bernasek, Surf. Sci. **163**, 215 (1985).
[13] D. W. Moon, S. L. Bernasek, D. J. Dwyer, and J. L. Gland, J. Am. Chem. Soc. **107**, 4363 (1985).
[14] D. W. Moon, S. L. Bernasek, J. P. Lu, J. L. Gland, and D. J. Dwyer, Surf. Sci. **184**, 90 (1987).
[15] S. D. Cameron and D. J. Dwyer, Langmuir **4**, 282 (1988).
[16] R. S. Saiki, G. S. Herman, M. Yamada, J. Osterwalder, and C. S. Fadley, Phys. Rev. Lett. **63**, 283 (1989).
[17] D. C. Sorescu, D. L. Thompson, M. M. Hurley, and C. F. Chabalowski, Phys. Rev. B **66**, 035416 (2002).
[18] J. Radnik, E. Chopovskaya, M. Grüne, and K. Wandelt, Surf. Sci. **352-354**, 268 (1996).
[19] Y. Tanabe, Y. Suzuki, T. Wadayama, and A. Hatta, Surf. Sci. **427-428**, 414 (1999); Y. Tanabe, T. Shibahara, R. Buckmaster, T. Ishibashi, T. Wadayama, and A. Hatta, Surf. Sci. **466**, 1 (2000).
[20] T. Wadayama, K. Kubo, T. Yamashita, T. Tanabe, and T. Hatta, Appl. Surf. Sci. **199**, 254 (2002).
[21] D. Spišák and J. Hafner, Phys. Rev. B **64**, 094418 (2001).
[22] D. J. Keavney, D. F. Storm, J. W. Freeland, I. L. Grigorov, and J. C. Walker, Phys. Rev. Lett. **74**, 4531 (1995).
[23] M.-T. Lin, J. Shen, W. Kuch, H. Jenniches, M. Klaua, C. M. Schneider, and J. Kirschner, Phys. Rev. B **55**, 5886 (1997).
[24] H. Li, Y. S. Li, J. Quinn, D. Tian, J. Sokolov, F. Jona, and P. M. Marcus, Phys. Rev. B **42**, 9195 (1990).
[25] B. Heinrich, K. B. Urquhart, J. R. Dutcher, S. T. Purcell, J. F. Cochran, A. S. Arrot, D. A. Steigerwald, and W. F. Egelhoff, Jr., J. Appl. Phys. **63**, 3863 (1988).
[26] V. Blum, C. Rath, S. Müller, L. Hammer, K. Heinz, J. M. García, J. E. Ortega, J. E. Priesto, O. S. Hernan, J. M. Gallego, A. L. Vazquez de Parga, and R. Miranda, Phys. Rev. B **59**, 15966 (1999).
[27] Ch. Hwang, A. K. Swan, and S. C. Hong, Phys. Rev. B **60**, 14 429 (1999).
[28] K. Hayashi, M. Sawada, A. Harasawa, A. Kimura, and A. Kakizaki, Phys. Rev. B **64**, 054417 (2001).
[29] K. Hayashi, M. Sawada, H. Yamagami, A. Kimura, and A. Kakizaki, Physica B **351**, 324 (2004).
[30] K. Hayashi, M. Sawada, H. Yamagami, A. Kimura, and A. Kakizaki, J. Phys. Soc. Jpn. **73**, 2550 (2004).
[31] C. Boeglin, H. Bulou, J. Hommet, X. Le Cann, H. Magnan, P. Le Fèvre, and D. Chandesris, Phys. Rev. B **60**, 4220 (1999).
[32] S.-K. Lee, J.-S. Kim, B. Kim, Y. Cha, W. K. Han, H. G. Min, J. Seo, and S. C. Hong, Phys. Rev. B **65**, 014423 (2001).
[33] T. C. Hufnagel, M. C. Kautzky, B. J. Daniels, and B. M. Clemens, J. Appl. Phys. **85**, 2609 (1999).
[34] C. Egawa, Y. Tezuka, S. Oki, and Y. Murata, Surf. Sci. **283**, 338 (1993).
[35] R. Pfandzelter, M. Lang, H. Winter, and I. Urazgildin, Surf. Rev. Lett. **10**, 117 (2003).
[36] C. Egawa, K. Onawa, H. Iwai, and S. Oki, Surf. Sci. **557**, 31 (2004).
[37] A. M. de Jong and J. W. Niemantsverdriet, J. Chem. Phys. **101**, 10126 (1994).
[38] W. A. Brown and D. A. King, J. Phys. Chem. B **104**, 2578

(2000).
[39] M. Gajdoš, A. Eichler, and J. Hafner, J. Phys.: Condens. Matter **16**, 1141 (2004).
[40] M. Gajdoš, J. Hafner, and A. Eichler, J. Phys.: Condens. Matter **18**, 13 (2006); **18**, 41 (2006).
[41] G. Kresse and J. Furthmüller, Phys. Rev. B **54**, 11 169 (1996); Comput. Mater. Sci. **6**, 15 (1996).
[42] P. E. Blöchl, Phys. Rev. B **50**, 17 953 (1994).
[43] G. Kresse and D. Joubert, Phys. Rev. B **59**, 1758 (1999).
[44] B. Hammer, L. B. Hansen, and J. K. Nørskov, Phys. Rev. B **59**, 7413 (1999).
[45] J. P. Perdew, J. A. Chevary, S. H. Vosko, K. A. Jackson, M. R. Pedersen, D. J. Singh, and C. Fiolhais, Phys. Rev. B **46**, 6671 (1992).
[46] J. P. Perdew, K. Burke, and K. Ernzerhof, Phys. Rev. Lett. **77**, 3865 (1999).
[47] P. Villars and L. D. Calvert, *Pearson's Handbook of Crystallographic Data for Intermetallic Phases*, 2nd ed. (ASM International, Materials Park, Ohio, 1991).
[48] E. Walker, J. Ashkenazi, and M. Dacorogna, Phys. Rev. B **24**, 2254 (1981).
[49] T. Takahashi, W. A. Bassetm, and H. K. Mao, J. Geophys. Res. **73**, 4717 (1968).
[50] D. L. Mills, Phys. Rev. B **3**, 3887 (1971).
[51] K. P. Huber and G. Herzberg, *Molecular Spectra and Molecular Structures IV, Constants of Diatomic Molecules* (Van Nostrand Reinhold, New York, 1979).
[52] M. Methfessel and A. T. Paxton, Phys. Rev. B **40**, 3616 (1989).
[53] B. T. Jonker, K. H. Walker, E. Kisker, G. A. Prinz, and C. Carbone, Phys. Rev. Lett. **57**, 142 (1986).
[54] M. A. Tomaz, D. C. Ingram, G. R. Harp, D. Lederman, E. Nayo, and W. L. O'Brien, Phys. Rev. B **56**, 5474 (1997).
[55] A. M. Begley, S. K. Kim, F. Jona, and P. M. Marcus, Phys. Rev. B **48**, 1786 (1993).
[56] E. G. Moroni, G. Kresse, J. Hafner and J. Furthmüller, Phys. Rev. B **56**, 15 629 (1997).
[57] D. Spišák and J. Hafner, Phys. Rev. B **70**, 014430 (2004).
[58] D. Spišák and J. Hafner, Phys. Rev. B **70**, 195426 (2004).
[59] S. Dennler and J. Hafner, Phys. Rev. B **72**, 214413 (2005).
[60] P. Ferriani, S. Heinze, G. Bihlmayer, and S. Blügel, Phys. Rev. B **72**, 024452 (2005).
[61] L. W. H. Leung and D. W. Goodman, J. Chem. Phys. **93**, 8328 (1990).
[62] A. M. de Jong and J. W. Niemandsverdriet, J. Chem. Phys. **101**, 10 126 (1994).
[63] A. Eichler and J. Hafner, J. Chem. Phys. **109**, 5585 (1998).
[64] W. Erley, J. Vac. Sci. Technol. **18**, 472 (1981).
[65] A. Stibor, G. Kresse, A. Eichler, and J. Hafner, Surf. Sci. **507-510**, 99 (2002); A. Stibor, Diploma Thesis, Universität Wien 2002 (unpublished).
[66] A. P. van Bavel, M. J. P. Hopstaken, D. Curulla, J. W. Niemantsverdriet, J. J. Lukkien, and P. A. J. Hilbers, J. Chem. Phys. **119**, 524 (2003).
[67] G. Blyholder, J. Chem. Phys. **68**, 2772 (1964).
[68] A. Nilsson, M. Weinelt, T. Wiell, P. Bennich, O. Karis, N. Wassdahl, J. Stohr, and M. G. Samant, Phys. Rev. Lett. **78**, 2847 (1997).